Predicting The Influence of Microvascular Structure On Tumour Response to Radiotherapy

James A. Grogan, Bostjan Markelc, Anthony J. Connor, Ruth J. Muschel, Joe M. Pitt-Francis, Philip K. Maini, and Helen M. Byrne

***Abstract*—*Objective*: The purpose of this study is to investigate how theoretical predictions of tumour response to radiotherapy depend on the morphology and spatial representation of the microvascular network. *Methods*: A hybrid multiscale model, that couples a cellular automaton model of tumour growth with a model for oxygen transport from blood vessels, is used to predict the viable fraction of cells following one week of simulated radiotherapy. Both artificial and biologically derived three-dimensional vessel networks of well vascularized tumours are considered and predictions compared with two-dimensional descriptions. *Results*: For literature-derived values of the cellular oxygen consumption rate there is little difference in predicted viable fraction when three-dimensional network representations of biological or artificial vessel networks are employed. Different two-dimensional representations are shown to either over- or under-estimate viable fractions relative to the three-dimensional cases, with predictions based on point-wise descriptions shown to have greater sensitivity to vessel network morphology. *Conclusion*: The predicted radiotherapy response is relatively insensitive to the morphology of the microvessel network when three-dimensional representations are adopted, however sensitivity is greater in certain two-dimensional representations. *Significance*: By using realistic three-dimensional vessel network geometries this study shows that real and artificial network descriptions and assumptions of spatially uniform oxygen distributions lead to similar radiotherapy response predictions in relatively small tissue volumes. This suggests that either a more detailed description of oxygen transport in the microvasculature is required or that the oxygen enhancement ratio used in the well known linear-quadratic radiotherapy response model is relatively insensitive to microvascular structure.**

***Index Terms*—Multiscale modelling, oxygen transport, vascular tumour growth, radiotherapy.**

I. Introduction

This project has received funding from the European Union's Seventh Framework Programme for research, technological development and demonstration under grant agreement No 600841. The research leading to these results has received funding from the People Programme (Marie Curie Actions) of the European Union's Seventh Framework Programme (FP7/2007-2013) under REA grant agreement No 625631. This work was also supported by Cancer Research UK (CR-UK) grant number C5255/A18085, through the CRUK Oxford Centre.

J.A. Grogan, P.K. Maini and H.M. Byrne are with the Mathematical Institute, University of Oxford, Oxford, UK; J.M. Pitt-Francis is with the Department of Computer Science, University of Oxford, Oxford, UK; A.J. Connor was with the Department of Computer Science, University of Oxford, Oxford, UK; B. Markelc and R.J. Muschel are with the Department of Oncology, CRUK/MRC Oxford Institute for Radiation Oncology, University of Oxford, Oxford, UK (correspondence e-mail: james.grogan@maths.ox.ac.uk).

Manuscript received May 18, 2016. Copyright (c) 2016 IEEE. Personal use of this material is permitted. However, permission to use this material for any other purposes must be obtained from the IEEE by sending an email to pubs-permissions@ieee.org.

IN *vitro* studies have shown that cancer cells in low oxygen environments have a greater probability of survival following radiotherapy than cells with greater oxygen availability [32]. This effect has been shown to translate to the clinic, with patients exhibiting markers for hypoxia having poorer radiotherapy response [5]. Oxygen availability in vascular tissue is closely linked with the function of the microvasculature and studies have focused on the measurements of vascular function [28] or microvessel density as indicators of radiotherapy responsiveness [11]. Important questions remain following these studies regarding the link between vascular structure, tumour tissue oxygenation and radiotherapy response. In particular, observations of improved radiotherapy outcome when vascular targeting agents are administered [12], suggest a temporal window during which the vascular structure can be optimized for tissue oxygenation as described by 'vascular normalization' theory [13].

Mathematical models of vascular tumour growth and radiation therapy response can be used to study the link between indirect measurements of vascular structure, tissue oxygenation and radiotherapy response. Dasu *et al.* [7], [8] have studied oxygenation profiles and radiotherapy response using planar tissue regions, a cellular automaton description of cells and a point-wise description of vessels. Vessels were heterogeneously distributed and predictions of different forms of the well known linear-quadratic (L-Q) model of cell survival, with and without an oxygen enhancement ratio (OER), were compared. The OER is used to represent the decrease in sensitivity of cells in low oxygen environments to radiotherapy. Scott *et al.* [29] used a similar approach to study the effects of spatial heterogeneity in the distribution of vessels on cell survival post-radiotherapy. The authors predicted that microvessel density alone does not adequately describe average tissue oxygenation or radiotherapy response and proposed improved spatial descriptions of heterogeneity in vessel spacing.

Many existing modelling studies focus on the *in vitro* response of tumour spheroids to radiotherapy [14], while models of the *in vivo* response neglect the vasculature [9] or they focus on the macroscale behaviour and neglect details of microvascular structure [26], [27]. Other authors have used detailed spatial descriptions of the microvascular network and oxygen transport processes to predict tissue oxygenation, without explicitly modelling cell response to radiotherapy [10], [23], [30], or they have adopted simplified or artificial descriptions of the vessel network and modelled cells discretely [16], [22], [24], [34]. The present study aims to investigate radiotherapy

response by retaining a discrete description of cell growth and treatment, while using realistic three-dimensional (3D) representations of biological vessel networks of well vascularized tumours. It is desirable to use a discrete description of cell growth and treatment response as this permits a more mechanistic description of the multiscale vascular tumour growth process. In particular, the approach allows a natural description of oxygen dependent cell cycling and radiotherapy survival at the cell scale and the simultaneous development of spatial heterogeneities in oxygen tension and cell populations as the nutrient is delivered from aberrant tumour vessels at larger spatial scales. The ability to represent spatial heterogeneities in oxygen tension and cellular composition is important when studying tumour response to radiotherapy, as it permits investigation of the processes that give rise to phenomena such as improved radiotherapy response following 'vessel normalization' and reduced responsiveness in hypoxic regions [12], [13].

In the present study a cellular automaton approach similar to those of Dasu *et al.* [7], Scott *et al.* [29] and Owen *et al.* [20] is used to simulate the growth of tumour cells. However, in this case a 3D tissue volume is considered and vessels are described as line sources of oxygen, rather than points. In addition, both artificial vessel networks and vessel networks derived from imaging data from mouse tumours are adopted. The inclusion of *in vivo* data on vessel network structures allows us to assess the ability of previously adopted artificial networks and two-dimensional (2D) descriptions, to predict radiotherapy outcome.

The remainder of the study is organised as follows. In Section 2 the vessel networks are introduced and methods for their construction described. Then the hybrid multiscale model of vascular tumour growth and cell response to radiotherapy is described and simulation test cases are introduced. In Section 3 numerical results are presented, showing predicted oxygen distributions and cell populations for each vessel network. Then, cell surviving fractions following the administration of one week of fractionated radiotherapy are generated and compared for each network. In Section 4 the key results are discussed, together with suggestions for future work. The paper concludes in Section 5 with a summary of our findings.

II. Methods

Predicted oxygen profiles and radiotherapy response are compared for simulated tumours with three different vessel networks, each with three different spatial representations. The networks are first introduced. Following this, the submodels of cell cycle progression and growth, oxygen delivery and consumption and radiation response are described. Finally, the algorithm used to generate numerical simulations is presented. All spatial dimensions are scaled relative to an assumed cell width, Δx, of 40 μm, as per Owen *et al.* [20].

A. Vessel Networks

Three vessel networks are studied, as shown in Fig. 1. The first, denoted 'Regular', is an artificial 2D regular hexagonal tessellation of a rectangular domain of dimension 40 x 40 cell widths. The network is positioned in the middle of a cuboidal domain with a depth of 7 cell widths. This network has previously been used in several studies of tumour growth and treatment [2], [3] and can be considered to represent a spatially homogeneous capillary bed. Three different spatial descriptions are studied; 'Slice', 'Planar' and '3D'. The '3D' description is obtained by randomly choosing the out-of-plane location of network branch points from a uniform distribution bounded by the domain depth. The 'Planar' description is obtained by projecting the network back onto the two-dimensional rectangular domain and the 'Slice' description is obtained by intersecting the '3D' description with the domain mid-plane. The intersection produces a collection of points and closely resembles the description of Dasu *et al.* [7] and Scott *et al.* [29].

The second network, denoted 'Random', is a 2D Voronoi tessellation bounded by a rectangular domain and with a uniform spatial distribution of point seeds. For the '3D' description vessel branch locations are perturbed randomly in the out-of-plane direction to fill the cuboidal domain. Following this, points are randomly selected from a normal distribution with mean centred at the domain midpoint. The closest vessels to these points are progressively removed until a target density is reached. The result, shown in Fig. 1(b), leads to a heterogeneous spatial distribution of vessels, with lower vessel density towards the centre of the domain. The 'Planar' and 'Slice' descriptions are obtained as previously described.

The third network, denoted 'Biological', is derived from a multi-photon image of a fluorescently labelled vessel network in a mouse tumour, as in Grimes *et al.* [10]. Briefly, murine colon adenocarcinoma (MC38) cells were cultured in Dulbecco's Modified Eagle Medium supplemented with 10% fetal bovine serum and 1% penicillin/streptomycin at 37 degress C in a humidified incubator with 5% CO_2. Tumours were induced by injecting 0.5 x 10^6 cells in 100 μL 1x phosphate buffered saline (PBS), injected subcutaneously onto the right flank of a 8-10 week old female C57/Bl6 mice (Charles River). When the tumour reached approximately 200 mm^3 in volume (calculated as length x width x height x $\pi/6$) anti-mouse CD31 PE labelled antibodies, specifically labelling endothelial cells, were injected intravenously (25 μg in 100 μL, BioLegend) to label perfused blood vessels. Mice were culled and tumours excised, cut in half and imaged 10 min after injection of labelled antibodies in a humidified chamber with a cover glass bottom with thickness of 0.17 mm. Images were acquired with a Zeiss LSM 880 microscope (Carl Zeiss AG), connected to a Mai-Tai tuneable laser (Spectra-Physics). Tumour tissue was excited with laser wavelength of 800 nm and the emitted light was collected on a Gallium Arsenide Phosphide (GaAsP) detector through a 562.5-587.5 nm band-pass filter for PE. A 20x water immersion objective with NA of 1.0 was used to acquire Zstacks-TileScan of a random region in the centre of tumour tissue with a pixel size of 0.83 μm in X and Y and a Z step of 2 μm. All animal studies were performed in accordance with the Animals Scientific Procedures Act of 1986 (UK) and Committee on the Ethics of Animal Experiments of the University of Oxford.

Following acquisition, image stacks were resized using bi-

linear interpolation in ImageJ [1] with pixel sizes increased by a factor of 4 in X and Y and 2 in Z. This operation facilitated later processing and also reduced noise. The channel containing the vessel label was converted to an 8-bit greyscale format and a binary mask was generated using thresholding with manual selection of upper and lower bounds (voxel intensities of 255 and 51 respectively). Vessel centre-lines were obtained from the mask using the Skeletonize3D "plug-in for ImageJ". Small vessels, with length $< 0.5\Delta x$, were removed from the network as they were deemed to be artefacts of the centre-line extraction. Vessel length distributions before and after removal are shown in Fig. 1(d). The network dimensions are 80 x 80 x 7 cell widths, and the domain is divided into four, equally sized sub-networks (see Fig. 1(c)). Subdivision is primarily for computational purposes, but also allows comparison of results in subregions of biological networks with different vessel distributions. Each sub-network is analysed individually and subject to the same 'Planar' and 'Slice' operations as the 'Random' network.

Vessel length density distributions are shown for the 'Biological' network, each sub-network and a sample of the artificial networks in Fig. 1(d). It is noted that the number of short vessels is greater in the biological networks than the artificial ones although, as shown in Fig. 1(e), average line densities are similar. It is also shown in Fig. 1(e) that line density increases significantly when a 2D 'Planar' representation is adopted. There is a significant variation in point density between the biological and artificial networks when the 2D 'Slice' representation is adopted, with the density being lower for the biological networks. This is due to the anisotropy of the biological network, which is not captured by the artificial networks and suggests that for this morphology multiple slices may need to be employed for point-based descriptions. The most suitable method for generating such slices is not considered in the present study, but the effect of the reduced point density due to using a single slice is investigated.

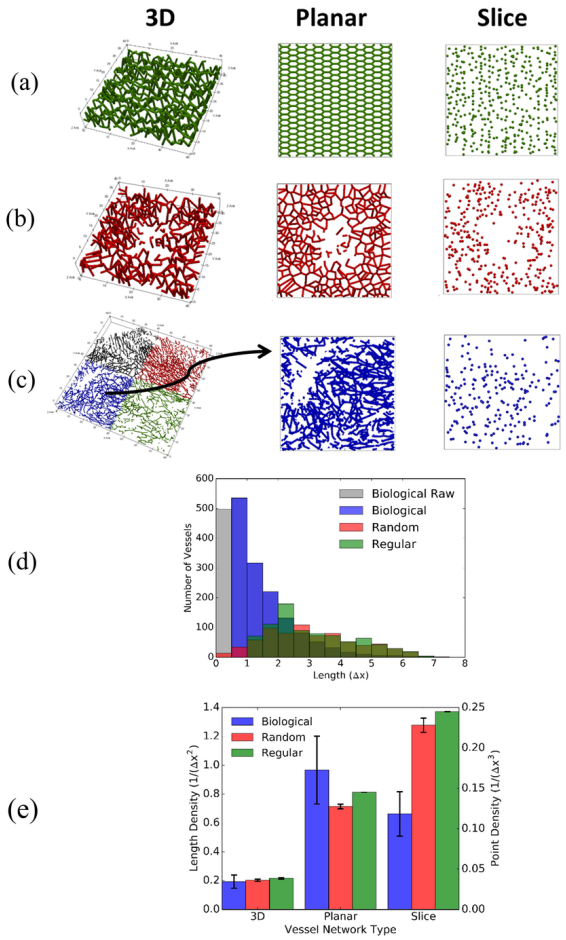


Fig. 1. The types of 3D and 2D vessel networks considered in this study. Plots show artificial networks with (a) 'Regular' and (b) 'Randomly' spaced vessels and (c) 'Biological' networks, with 3D and 2D 'Planar' and 'Slice' representations. (d) The distribution of vessel lengths for the 3D networks. 'Biological Raw' is the distribution before short vessels removal. (e) The average length density for the 3D and 2D 'Planar' networks, and the average point density of vessels for the 2D 'Slice' networks. Error bars denote one standard deviation, with artificial networks generated using different random seeds and the biological network divided into four sub-networks.

B. Model Overview

The multiscale model of tumour growth and radiation treatment response adopted in this study is shown in Fig. 2. Cells are modelled discretely, using a cellular automaton approach. Three cell states are considered, 'Normoxic', 'Quiescent' and 'Apoptotic'. In a pre-processing step a regular grid of spacing equal to an assumed (biological) cell spacing of Δx is generated, filling the cuboidal simulation domain. All sites on the grid are populated with 'Normoxic' cancer cells, except those occupied with a vessel. Vessels are described using a lattice-free approach, but vessel positions are interpolated onto the regular cell grid and the finite-difference grid used to solve the partial differential equation (PDE) governing tissue oxygen levels. The PDE governing tissue oxygen levels is of the form:

$$D_e \nabla^2 c - \delta(\mathbf{x}) k c = 0, \tag{1}$$

where c is the oxygen tension, D_e is the effective oxygen diffusion coefficient, and k is the rate of oxygen consumption per cell [20]. The delta function $\delta(\mathbf{x})$ is unity at cell centres and zero elsewhere. No flux of oxygen is permitted through any of the planar faces of the bounding cuboid. Vessels act as constant sources of oxygen. Each point on the PDE grid which coincides with a vessel is prescribed a fixed oxygen tension of 30 mmHg, by means of a point-wise Dirichlet boundary condition.

Following the model pre-processing steps the cell population and oxygen field are updated at each time increment, of duration 1.0 hour, while the vasculature is static. The detailed cell update is shown in Fig. 3. 'Normoxic' cells pass through a cell cycle, according to a model described in detail in Owen *et al.* [20]. In particular, a scalar parameter $0 \leq \phi \leq 1$ is used to describe a cell's progress through its cycle via

$$\frac{d\phi}{dt} = \frac{1}{T_{min}} \frac{c}{(c_\phi + c)}, \tag{2}$$

where the cycle starts at $\phi = 0$ and ends, with attempted division, when $\phi = 1$, T_{min} is the minimum period of the

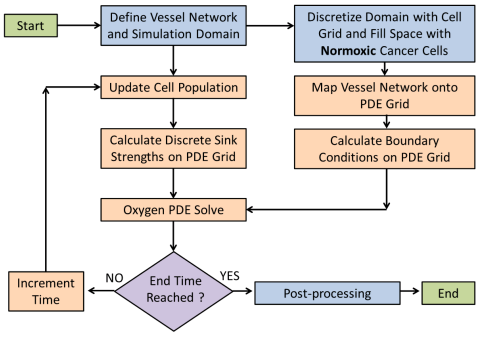


Fig. 2. Flowchart of the algorithm used in numerical simulations of the hybrid, multiscale model of tumour growth and response to radiotherapy.

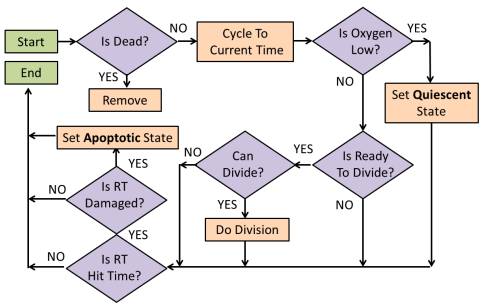


Fig. 3. Schematic of the algorithm used to update the cell population on each timestep, including radiotherapy (RT) administration.

cell cycle in oxygen rich conditions and c_ϕ is the oxygen tension at which the rate of progression through the cycle is half-maximal. Cells become quiescent and no longer cycle if the oxygen tension falls below a threshold value ($c < c_q^i$). Quiescent cells may resume cycling if the oxygen tension increases sufficiently ($c > c_q^o$). If a cell remains quiescent for a time period greater than the threshold T_q, then it becomes apoptotic. When radiotherapy is delivered, a fraction of the proliferating cells ($1 - SF$) become apoptotic, where SF, the survival fraction, depends on the local oxygen tension c in the following way:

$$SF = e^{-\alpha D - \beta D^2}, \tag{3}$$

where D is the radiation dose (in Gy) and $\alpha = \alpha(c)$ and $\beta = \beta(c)$ are empirical, oxygen-dependent parameters given by:

$$\alpha(c) = \frac{\alpha_{max}}{OER_\alpha(c)}, \quad \beta(c) = \frac{\beta_{max}}{OER_\beta(c)}, \tag{4}$$

and the OER satisfies [21]

$$OER(c) = OER_{min} + (OER_{max} - OER_{min})\frac{K_{OER}}{c + K_{OER}}. \tag{5}$$

where OER_{min}, OER_{max} and K_{OER} are empirical constants. Apoptotic cells are set to a 'Dead' state and no longer occupy space after a period of 30 hours. The viable fraction of cells at time t, $VF(t)$, is defined to be the total number of 'Normoxic' and 'Quiescent' cells at time t divided by the total number of cells at the start of the simulation ($t = 0$). This quantity is a model output, which is distinct from the SF which is a model input, and includes loss of cells due to both radiotherapy and hypoxia.

C. Study Overview

Tumour growth and radiotherapy were simulated for each of the three types of vessel network and for each of the three spatial representations of the vessel networks, using as default the parameter values stated in Table 1. For comparison, control cases with no vessels ($c = 0$ mmHg at all points, 'Low') and well oxygenated tissue ($c = 30$ mmHg at all points, 'High') were also simulated. For all cases, five realisations of the 'Random' network and five realisations of the 3D 'Regular' network were simulated. Additionally, radiotherapy ($D = 2$ Gy) was administered at $t = 2$ hours and thereafter every 24 hours over a period of five days. Treatment was then halted and the tumour allowed to re-grow for a total simulation time of 200 hours (just over 8 days).

In all cases the number of cells in each state and the mean cell oxygen tensions were recorded every five hours, with a simulation time increment of one hour and cell cycle time increment of 30 minutes adopted. Simulations were built using the C++ Chaste library [17] with Python based bindings and post-processing, ordinary differential equation systems were solved using CVODE [6] and PDE systems using a finite-difference scheme implemented with PETSc tools [4]. Simulation clock time was between 30 seconds and five minutes on a single AMD-FX4350 processor.

TABLE I
SUMMARY OF MODEL PARAMETERS AND ESTIMATES OF THEIR VALUES

Parameter	Symbol	Units	Value	Source
Effective Diffusivity	D_e	$cm^2 min^{-1}$	0.00145	[20]
Oxygen Consumption Rate	k	min^{-1}	13	[20]
Radiotherapy Dose	D	Gy	2.0	-
Radiotherapy Parameter	α_{max}	Gy^{-1}	0.3	[7]
Radiotherapy Parameter	β_{max}	Gy^{-2}	0.03	[7]
Oxygen Enhancement Parameter	$OER_{\alpha,min}$	-	1	[29]
Oxygen Enhancement Parameter	$OER_{\alpha,max}$	-	1.75	[29]
Oxygen Enhancement Parameter	$OER_{\beta,min}$	-	1	[29]
Oxygen Enhancement Parameter	$OER_{\beta,max}$	-	3.25	[29]
Oxygen Enhancement Parameter	K_{OER}	mmHg	3.28	[29]
Minimum Cell Cycle Duration	T_{min}	min	1600	[20]
Cell Cycle Rate Constant	c_ϕ	mmHg	1.4	[20]
Quiescence Entrance Threshold	c_q^i	mmHg	8.9	[20]
Quiescence Exit Threshold	c_q^o	mmHg	9.8	[20]
Maximum Quiescence Duration	T_q	min	4000	[20]

III. Results

A. Cell Growth and Response to Radiotherapy

Typical simulation results for the 3D and 2D biological networks are presented in Fig. 4 and the associated summary statistics are plotted in Fig. 5. Prior to radiotherapy, the 3D tissue is densely populated with tumour cells which consume oxygen. As a result, the tissue is characterised by large regions with low oxygen and smaller, well-oxygenated regions. When radiotherapy is administered, due to the OER, well-oxygenated cells are killed at a greater rate than the poorly-oxygenated ones. As the tumour burden decreases, average oxygen levels rise and, as a result, the remaining cells become more vulnerable to radiotherapy. After 200 hours (and 5 rounds of radiotherapy), the tumour cells repopulate the domain, causing the survival fraction (see Equation (3)) to increase. The results for the 2D simulations are similar, with progressively more tumour cell death for the 2D 'Planar' and 'Slice' network representations. Given that the 2D 'Planar' network is better oxygenated than its 3D counterpart, this suggests that, for the parameter values being used, the amount of cell death caused by radiotherapy is so great that it takes longer for the cells associated with the 2D 'Planar' network to repopulate the tissue than for the 3D case where lower oxygen levels reduce the cell proliferation rate but have a stronger, inhibitory effect on radiosensitivity. An additional anomaly associated with the 2D 'Planar' representation is that tumour cells and their progeny must remain localised in finite regions surrounded by blood vessels. If all the tumour cells in one such region are eliminated following radiotherapy then that region will ever after remain devoid of tumour cells: this is not the case for the 2D 'Slice' or 3D network representations.

B. Effect of Vessel Morphology on Response to Radiotherapy

The results presented in Fig. 5 reveal that, in 3D, details of the microstructure of the vessel network have a negligible effect on the tumour's growth dynamics and/or its response to radiotherapy. There is good agreement between the predicted evolution of the average oxygen tension and the fraction of viable cells for 3D simulations using the 'Biological', 'Random' and 'Regular' networks. In particular, when the oxygen consumption rate is low (Fig. 5(a,b,c)) the system dynamics can be accurately approximated by the 'High' control case for which oxygen levels at all times are maintained at the same high levels throughout the tissue domain. Slight functional discrepancies between the different networks become apparent when the oxygen consumption rate is high (Fig. 5(d,e,f)). In this case, the biological network is typically better oxygenated than the synthetic ones, as shown in Fig. 5(d). It also has a lower proportion of hypoxic cells (Fig. 5(c)) and, once radiotherapy stops, regrows more rapidly as shown in Fig. 5(f).

C. Effect of Vessel Representation on Response to Radiotherapy

The simulation results in Fig. 4 suggest that, for the biological network, the 2D 'Planar' representation does not accurately represent the 3D one. These comparisons are made more precise in Fig. 6 where we plot the viable fraction, VF(t), at two time points (t=5, 95 hours) for all vessel networks and two oxygen consumptions.

At early times, when the oxygen consumption rate is low, VF(t) increases as the geometry changes from 3D to 2D 'Planar' and 2D 'Slice' for the 'Biological', 'Random' and 'Regular' networks, and a similar trend is seen for the two control cases (see Fig. 6(a)). Since for the control cases, oxygen levels are identical for the 3D and 2D geometries, we ascribe this trend to undersampling: the 2D domains contain significantly fewer cells than the 3D domains so, for the 2D simulations, there are fewer cells to sample when deciding whether a particular cell will survive radiotherapy. In future work, we will investigate this claim further by performing simulations on larger domains.

As the oxygen consumption rate increases (Fig. 6(b)), or at later times (Fig. 6(c)), the influence of geometry on the cells' response to radiotherapy becomes more apparent. Relative to a particular 3D network, the 'Slice' representation overestimates the VF whereas the 'Planar' representation underestimates it. Fig. 4 reveals that these differences are due to the 'Planar' ('Slice') representation supplying more (less) oxygen to the cells than the 3D representation and, thereby, increasing (decreasing) the cell kill rate on exposure to radiotherapy.

An interesting anomaly is observed between the 3D and 2D 'Slice' network representations. At early times (5 hours), average hypoxic fractions for the 2D 'Slice' (0.41) are significantly higher for the 'Biological' network than for the 3D representation (0.17). Fractions in the 'Random' network are similar for the 'Slice' (0.18) and 3D case (0.20), while fractions in the 'Regular' network are underestimated in the 'Slice' (0.05) relative to the 3D case (0.20). Although the hypoxic fractions are quite different, the predicted mean oxygen tensions in each representation are reasonably similar (9.0 mmHg, 13.9 mmHg and 16.3 mHg for the 'Slice' representation of the 'Biological', 'Random' and 'Regular' networks respectively and 14.2 mmHg, 12.9 mmHg and 11.5 mmHg for the corresponding 3D representations). The greater hypoxic fraction in the 2D 'Biological' network leads to a reduced initial radiotherapy response, as shown in Fig. 7, followed by a rapid reduction in VF as hypoxic cells start to die at $t \simeq 60$ hours. This is the timescale associated with apoptosis of the quiescent cells that the low oxygen environment creates. The additional cell death due to oxygen deprivation results in the considerably lower viable fraction predicted by the 'Slice' representation of the 'Biological' network than the others, as shown in Fig. 6(d). This greater hypoxic fraction in the 'Slice' network may be due to heterogeneity in the vessel spacing, which is most evident in the 'Biological' network. The predictions of the 2D 'Slice' representation thus appear to have greater sensitivity to spatial heterogeneity in the vessel distribution than the 3D representation.

IV. Discussion

We have used a hybrid, multiscale model to investigate how the representation of microvascular networks influences tissue oxygenation and the response of tumours to multiple

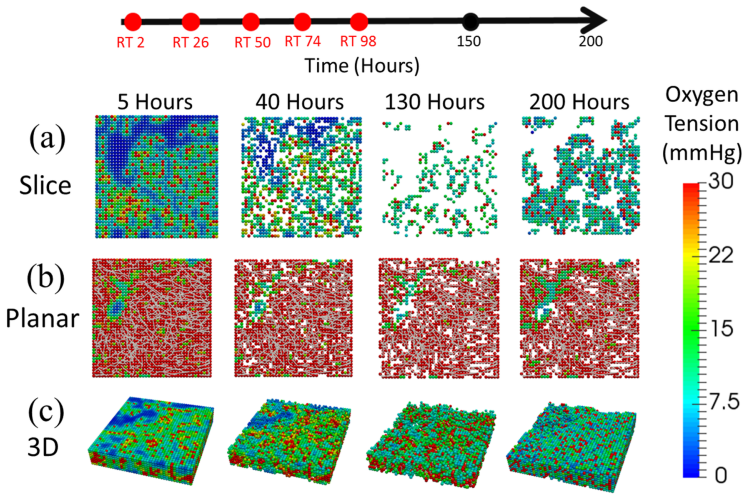


Fig. 4. Influence of geometry on cell growth and response to radiotherapy. Simulations at times t = 5, 40, 130 and 200 hours, comparing the response of tumour cells embedded in (a) 'Slice', (b) 'Planar' and (c) the '3D' representation of one of the biological networks to 5 rounds of daily radiotherapy (RT). Administration times are also indicated. Cellular oxygen tension in mmHg is contoured. Parameter values: as per Table 1, except for the oxygen consumption rate which is increased by a factor of 15 (from $k = 13$ min^{-1} to $k = 195$ min^{-1}).

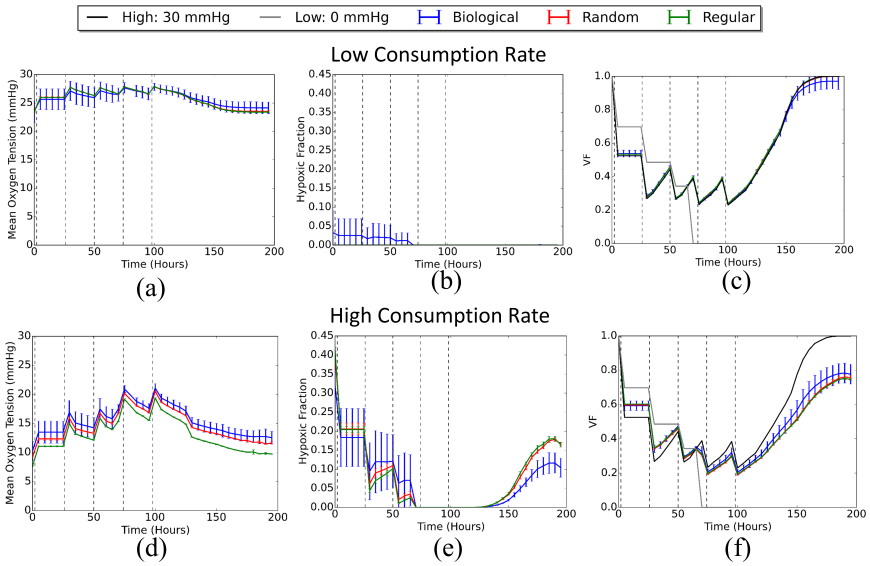


Fig. 5. Influence of vessel network representation on tumour cell growth and response to radiotherapy. Subplots show (a) the predicted mean cell oxygen tension, (b) hypoxic fraction of cells ($c < 5$ mmHg) and (c) viable fraction of cells over time, respectively, for the lower oxygen consumption rate ($k = 13$ min^{-1}) in 3D vessel networks. Subplots (d), (e) and (f) show the corresponding results for a consumption rate which is 15 times higher ($k = 195$ min^{-1}). Also included are results from 'Low' and 'High' controls where oxygen tensions are held fixed at 0 mmHg and 30 mmHg respectively at all points in the domain. The vertical dashed lines indicate radiotherapy administration times.

rounds of radiotherapy. Numerical simulations in 3D reveal no significant differences for the three network types under consideration, although it is noted that the studied biological network is relatively well vascularized. If oxygen consumption rates are low, then details of the microvascular structure in the case of well vascularized tumours can be ignored and the tumour's growth dynamics and response to radiotherapy is reasonably predicted by assuming that tissue oxygen levels are constant in space and time. As the oxygen consumption rate increases, this approximation ceases to apply as mean oxygen levels change over time (see Figs. 5(a) and (d)). Based on these results, we conclude that, when predicting tumour growth and response to radiotherapy, details of the vasculature supplying oxygen to the tumour should be taken into consideration but that biological structure for this well vascularized case can be reasonably approximated by an equivalent 'Random' or 'Regular' network.

Our 3D simulations provide a detailed description of oxygen transport in tumour regions that are small (1.6mm × 1.6mm × 0.28 mm) relative to human tumour sizes. In practice, when simulating the treatment of patients in the clinic, larger tissue regions should be considered. Homogenisation techniques can

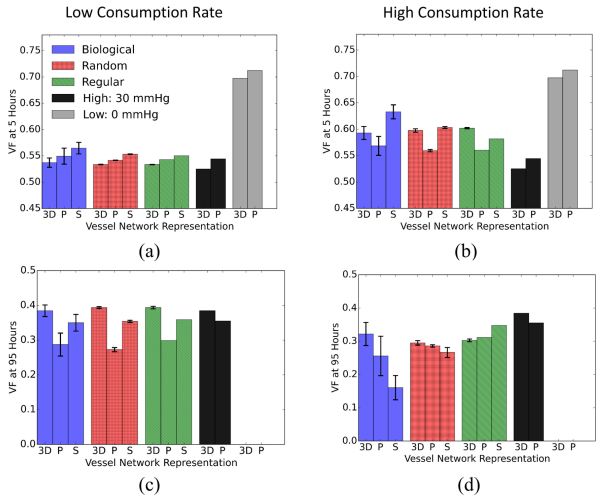


Fig. 6. Influence of geometry and vessel network representation on tumour response to radiotherapy. Cell survival fractions at t = 5 hours for (a) the default oxygen consumption rate (k = 13 min^{-1}) and (b) a high oxygen consumption rate (k = 195 min^{-1}). The corresponding results at t = 95 hours are presented in (c) and (d). Key: 3D-'3D' Network, P-'Planar', S-'Slice'.

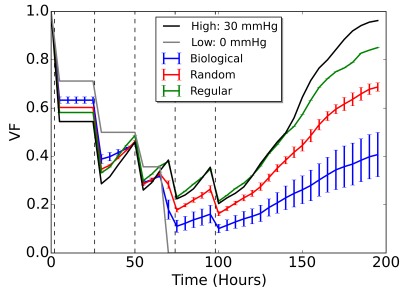


Fig. 7. Predicted cell viable fraction for the 2D 'Slice' vessel network. The vertical dashed lines indicate radiotherapy administration times. Parameter values: as per Table 1, except oxygen consumption rate which is fixed at a high level (k = 195 min^{-1}).

be used to relate bulk or macroscale properties of vascular tumours to their microscale structure [31]. Our analysis reveals that assuming a regular or periodic distribution of vessels at the microscale, which greatly simplifies the upscaling analysis, will yield predictions for oxygen transport at the tissue scale which will be similar to those generated from the underlying biological network.

Comparison of simulation results for the 3D and 2D geometries suggests that care is needed when extrapolating results from 2D approximations to 3D. In more detail (and as illustrated in Figs. 4 and 5), the 2D 'Slice' representations of the networks tend to overestimate viable tumour cell numbers at early times and to underestimate them at later times. By contrast, the 2D 'Planar' representation of the vessel networks consistently overestimates the cell kill following radiotherapy. There are several reasons for these discrepancies. First, the vessel volume fraction associated with 2D 'Planar' representations overestimates that of the 3D network while the 2D 'Slice' representation underestimates it. For the 2D 'Planar' representation, when vascular remodelling or multiple occupancy for lattice points [20] are neglected, tumour cells may get trapped in sub-regions of the tissue that are enclosed by blood vessels - if all tumour cells in such a region are eliminated, that region will always remain devoid of tumour cells.

Our results correspond to relatively small tumour regions (less than 1mm^3) which are reasonably homogeneous, due to the choice of cell line and use of a mouse model. When studying tumour growth in humans, larger tissue regions should be considered and these may encompass larger scale (intratumoral) heterogeneities, with subregions of hypoxia, necrosis and normoxia coexisting in a given tissue region. Scott *et al.* [29] studied larger tissue regions in a similar study and predicted that at low vessel densities, radiation efficacy decreased when the vessels were uniformly distributed whereas at high vessel densities, while radiation efficacy increased when vessels were uniformly distributed. We conclude that when relating macroscale properties of tumour tissue to microscale features, a key challenge is correctly defining the size of the microscale regions. It is noted from Fig. 6 (d) that the predicted viable fraction in the 2D 'Slice' representations is more sensitive to heterogeneities in the vessel distribution between the 'Regular' and 'Random' networks than the 3D representations. This suggests that further study is also required into the sensitivity of point-wise representations of vessel networks to spatial heterogeneities relative to 3D descriptions.

The relatively sparse cell spacing of 40 μm used in this study should be reduced to more closely resemble the packing of cancer cells in 3D, as is investigated in the study of Owen *et al.* [20], who allowed for multiple cell occupancy at lattice sites. This is feasible with the present model, as with careful interpolation of vessel locations onto the regular lattice, simulation times are expected to scale approximately linearly with cell number. It is noted however, that one of the main outcomes of such a spatially uniform increase in cell numbers is an increased average oxygen consumption rate. This has already been explored in the present study by increasing the oxygen consumption rate by a factor of 15. Some further insights into how predictions depend on model inputs in Table 1 can be gained based only on this change in oxygen consumption rate. For example, parameters increasing the drop in oxygen tension between vessels, or dependence of radiotherapy surviving fraction on oxygen tension, are expected to exacerbate differences in predicted viable fractions post radiotherapy. A more formal, global, sensitivity analysis [15] would be beneficial for a more detailed exploration of the role of parameters in Table 1 and to assess prediction robustness to parameter changes. This should be feasible given the relatively short simulation times in this study, but is postponed to future work.

Like Scott *et al.* [29], our simulation results are derived from static vascular networks that supply oxygen to the tumour tissue at a constant rate. In future work, we will investigate how our results change when effects such as tumour blood flow, angiogenesis and vascular remodelling are incorporated. While models of these processes have been implemented in existing multiscale models of vascular tumour growth (for

example [16], [19], [20]), they have not been validated against suitable experimental data. In future work, we aim to use *in vitro* and *in vivo* measurements of red blood cell transport through realistic tumour networks and measurements of micro-vasculature evolution [25], [33] to develop and validate mathematical models for these processes. We will use the validated models to investigate the impact of vessel normalisation strategies on tumour responses to radiotherapy [13] and to determine how different treatments (*e.g.* chemotherapy and immunotherapy) should be coordinated with radiotherapy and personalised for individual patients.

V. Conclusion

We have implemented a hybrid, multiscale model of vascular tumour growth and used it to investigate how the microscale description of the vessel network influences tissue oxygenation and the tumour's response to radiotherapy. No significant differences in either tissue oxygen levels or tumour burden were observed when 3D simulations were generated from 'Biological', 'Random' and 'Regular' vessel networks. Tumour growth dynamics in each case were in good agreement with results generated from simulations in which a spatially uniform oxygen distribution was imposed across the tissue domain. Comparison of results from 3D and 2D simulations revealed that 2D 'Slices' through the 3D vasculature provide a better approximation to the 3D network than 2D 'Planar' representations. This is because oxygen tension is not overestimated and lattice occupancy artefacts are not introduced. However, 'Slices' overestimated cell death in certain cases when oxygen consumption rates were high. Implicit in these conclusions are two key modelling assumptions: (i) oxygen levels are maintained at constant levels at all points within the vessel network, and (ii) the vessel network is not subject to remodelling. Future work is focused on relaxing these assumptions, with the ultimate aim of establishing how vessel normalisation strategies should be administered to maximise the therapeutic efficacy of radiotherapy.

References

[1] M.D. Abramoff, "Image processing with ImageJ," *Biophotonics International*, vol. 11, no. 7, pp. 36-42, 2004.

[2] T. Alarcon, "A cellular automaton model for tumour growth in inhomogeneous environment," *Journal of Theoretical Biology*, vol. 225,, no. 2, pp. 257-74, 2003.

[3] T. Alarcon, "A multiple scale model for tumor growth," *Multiscale Modeling and Simulation*, vol. 3, no. 2, pp. 440-475, 2005.

[4] S. Balay, "PETSc users manual revision 3.5. Technical Report," *Argonne National Laboratory (ANL)*, 2014.

[5] A.C. Begg, "Predicting recurrence after radiotherapy in head and neck cancer," *Seminars in Radiation Oncology*, vol. 22, no. 2, pp. 108-118, 2012.

[6] S.D. Cohen and A.C. Hindmarsh, "PCVODE, a stiff/nonstiff ODE solver in C," *Computers in Physics*, vol. 10, no. 2, pp. 138-43, 1996

[7] A. Dasu, "Theoretical simulation of tumour oxygenation and results from acute and chronic hypoxia," *Physics in Medicine and Biology*, vol. 48, no. 17, p. 2829, 2003.

[8] A. Dasu, "The effects of hypoxia on the theoretical modelling of tumour control probability," *Acta Oncologica*, vol. 44, no. 6, pp. 563-571, 2005.

[9] H. Enderling, "Quantitative modelling of tumour dynamics and radiotherapy," *Acta Biotheoretica,* vol. 58, no. 4, pp. 341-353, 2010.

[10] D.R. Grimes, "Estimating oxygen distribution from vasculature in three-dimensional tumor tissue," *Journal of The Royal Society Interface*, vol. 13, no. 116, p20160070, 2016.

[11] L. Hlatky, "Clinical application of antiangiogenic therapy: microvessel density, what it does and doesn't tell us," *Journal of the National Cancer Institute*, vol. 94, no. 12, pp. 883-893, 2002.

[12] M.R. Horsman and J. Overgaard, "The impact of hypoxia and its modification of the outcome of radiotherapy," *Journal of Radiation Research*, [Epub ahead of print], 2016.

[13] R.K. Jain, "Normalisation of tumour vasculature: an emerging concept in antiangiogenic therapy," *Science*, vol. 307, no. 5706, pp. 58-62, 2005.

[14] H. Kempf, "Spatio-temporal cell dynamics in tumour spheroid irradiation," *The European Physical Journal D,* vol. 60, no. 1, pp. 177-193, 2010.

[15] S. Marino, "A methodology for performing global uncertainty and sensitivity analysis in systems biology," *Journal of Theoretical Biology*, vol. 254, no. 21, pp. 178-196, 2008.

[16] S.R. McDougall, "Mathematical modelling of flow through vascular networks: implications for tumour-induced angiogenesis and chemotherapy strategies," *Bulletin of Mathematical Biology*, vol. 64, no. 4, pp. 673-702, 2002.

[17] G.R. Mirams, "Chaste: an open source C++ library for computational physiology and biology," *PLoS Computational Biology*, vol. 9, no. 3, p. e1002970, 2013.

[18] J. Overgaard and M.R. Horsman, "Modification of hypoxia-induced radioresistance in tumours by the use of oxygen and sensitizers," *Seminars in Radiation Oncology*, vol. 6, no. 1, pp. 10-21, 1996.

[19] M.R. Owen, "Angiogenesis and vascular remodelling in normal and cancerous tissues," *Journal of Mathematical Biology*, vol. 58, nos. 4-5, pp. 689-721, 2009.

[20] M.R. Owen, "Mathematical modelling predicts synergistic antitumour effects of combining a macrophage-based, hypoxia-targetted gene therapy with chemotherapy," *Cancer Research,* vol. 71, no. 8, pp. 2826-2837, 2011.

[21] B. Palcic and L.D. Skarsgard, "Reduced oxygen enhancement ratio at low doses of ionizing radiation" *Radiat Res.,* vol. 100, no. 2, pp. 328-339, 1984.

[22] H. Perfahl, "Multiscale modelling of vascular tumour growth in 3D: the roles of domain size and boundary conditions," *PLoS One*, vol. 6, no. 4, p. e14790, 2011.

[23] A.S. Popel, "Analysis of capillary-tissue diffusion in multicapillary systems," *Mathematical Biosciences*, vol. 39, pp. 187-211, 1978.

[24] G.G. Powathil, "Towards predicting the response of a solid tumour to chemotherapy and radiotherapy treatments: clinical insights from a computational model." *PLoS Comp. Biol.,* vol. 9, no. 7, p. e1003120, 2013.

[25] A.R. Pries, "Blood flow in microvascular networks. Experiments and simulation," *Circulation Research*, vol. 67, no. 4, pp. 826-834, 1990.

[26] R. Rockne, "A mathematical model for brain tumour response to radiation therapy," *Journal of Mathematical Biology,* vol. 58, nos. 4-5, pp. 561-578, 2009.

[27] R.C. Rockne, "A patient-specific computational model of hypoxia-modulated radiation resistance in glioblastoma using 18F-FMISO-PET," *Journal of the Royal Society Interface*, vol. 12, no. 103, p. 20141174, 2015.

[28] K.E. Schlageter, "Microvessel organisation and structure in experimental brain tumours: microvessel populations " *Microvascular Research*, vol. 58, no. 3, pp. 312-328, 1999.

[29] J.G. Scott, "Spatial metrics of tumour vascular organisation predict radiation efficacy in a computational model," *PLOS Computational Biology*, vol. 12, no. 1, p. e1004712, 2016.

[30] T.W. Secomb, "Analysis of oxygen transport to tumor tissue by microvascular networks," *International Journal of Radiation Oncology Biology Physics*, vol. 25, no. 3, pp. 481-489, 1993.

[31] R.J. Shipley and S.J. Chapman, "Multiscale modelling of fluid and drug transport in vascular tumours," *Bulletin of Mathematical Biology*, vol. 72, no. 6, pp. 1464-1491, 2010.

[32] R.M. Sutherland and R.E. Durand, "Radiation response of multicell spheroids – an in vitro tumour model," *Current Topics in Radiation Research Quarterly*, vol. 11, no. 1, pp. 87-139, 1976.

[33] G.M. Tozer, "Intravital imaging of tumour vascular networks using multi-photon fluorescence microscopy," *Advanced Drug Delivery*, vol. 57, pp. 135-152, 2005.

[34] M. Welter and H. Rieger, "Physical determinants of vascular network remodeling during tumor growth," *The European Physical Journal E, Soft matter*, vol. 33, no. 2, pp. 149-163, 2010.